2016

Precise methane absorption measurements in the 1.64 mu m spectral region for the MERLIN mission

T. Delahaye
Univ Paris Diderot, Univ Paris Est Creteil, Inst Pierre Simon, CNRS,LISA,UMR 7583, Creteil, France;

H. Tran
Univ Paris Diderot, Univ Paris Est Creteil, Inst Pierre Simon, CNRS,LISA,UMR 7583, Creteil, France;

S. E. Maxwell
NIST, Gaithersburg, MD 20899 USA;

V. M. Devi
College of William and Mary, Dept Phys, Williamsburg, VA 23185 USA

Recommended Citation

Delahaye, T., Maxwell, S. E., Reed, Z. D., Lin, H., Hodges, J. T., Sung, K., ... & Tran, H. (2016). Precise methane absorption measurements in the 1.64 μm spectral region for the MERLIN mission. Journal of Geophysical Research: Atmospheres, 121(12), 7360-7370.

AGU PUBLICATIONS

JGR

Journal of Geophysical Research: Atmospheres

RESEARCH ARTICLE
10.1002/2016JD025024

Key Points:
- We present a high-precision measurement of methane absorption in the 1.64 μm spectral region for the MERLIN mission
- High-resolution and high signal-to-noise absorption spectra of methane in air were recorded using a frequency-stabilized CRDS apparatus
- Obtained data and model allow for the calculation of CH_4 absorptions with a precision of better than 0.1% at the online position of MERLIN

Correspondence to:
H. Tran,
ha.tran@lisa.u-pec.fr

Citation:
Delahaye, T., S. E. Maxwell, Z. D. Reed, H. Lin, J. T. Hodges, K. Sung, V. M. Devi, T. Warneke, P. Spietz, and H. Tran (2016), Precise methane absorption measurements in the 1.64 μm spectral region for the MERLIN mission, *J. Geophys. Res. Atmos.*, *121*, 7360–7370, doi:10.1002/2016JD025024.

Received 3 MAR 2016
Accepted 31 MAY 2016
Accepted article online 2 JUN 2016
Published online 18 JUN 2016

Precise methane absorption measurements in the 1.64 μm spectral region for the MERLIN mission

T. Delahaye[1], S. E. Maxwell[2], Z. D. Reed[2], H. Lin[2,3], J. T. Hodges[2], K. Sung[4], V. M. Devi[5], T. Warneke[6], P. Spietz[7], and H. Tran[1]

[1]Laboratoire Interuniversitaire des Systèmes Atmosphériques (LISA, CNRS UMR 7583), Université Paris Est Créteil, Université Paris Diderot, Institut Pierre-Simon Laplace, Créteil, France, [2]National Institute of Standards and Technology, Gaithersburg, Maryland, USA, [3]National Institute of Metrology, Beijing, China, [4]Jet Propulsion Laboratory, California Institute of Technology, Pasadena, California, USA, [5]Department of Physics, College of William and Mary, Williamsburg, Virginia, USA, [6]Institute of Environmental Physics, University of Bremen, Bremen, Germany, [7]DLR German Aerospace Center, Institute of Space Systems, Bremen, Germany

Abstract In this article we describe a high-precision laboratory measurement targeting the R(6) manifold of the $2\nu_3$ band of $^{12}CH_4$. High-fidelity modeling of this absorption spectrum for atmospheric temperature and pressure conditions will be required by the Franco-German, Methane Remote Sensing LIDAR (MERLIN) space mission for retrievals of atmospheric methane. The analysis uses the Hartmann-Tran profile for modeling line shape and also includes line-mixing effects. To this end, six high-resolution and high signal-to-noise ratio absorption spectra of air-broadened methane were recorded using a frequency-stabilized cavity ring-down spectroscopy apparatus. Sample conditions corresponded to room temperature and spanned total sample pressures of 40 hPa–1013 hPa with methane molar fractions between 1 μmol mol^{-1} and 12 μmol mol^{-1}. All spectroscopic model parameters were simultaneously adjusted in a multispectrum nonlinear least squares fit to the six measured spectra. Comparison of the fitted model to the measured spectra reveals the ability to calculate the room temperature, methane absorption coefficient to better than 0.1% at the online position of the MERLIN mission. This is the first time that such fidelity has been reached in modeling methane absorption in the investigated spectral region, fulfilling the accuracy requirements of the MERLIN mission. We also found excellent agreement when comparing the present results with measurements obtained over different pressure conditions and using other laboratory techniques. Finally, we also evaluated the impact of these new spectral parameters on atmospheric transmissions spectra calculations.

1. Introduction

Methane (CH_4) is the second most important anthropogenic greenhouse gas after carbon dioxide. It is responsible for about 20% of the warming induced by long-lived greenhouse gases [*Kirschke et al.*, 2013]. Since preindustrial times, the background molar fraction of atmospheric methane has increased approximately 2.5 times to its present value of 1.8 μmol mol^{-1}. Methane emissions are caused by human activities as well as natural sources [*Kirschke et al.*, 2013]. The lack of precise global measurements of atmospheric methane is a major problem which limits our understanding of methane source and sink processes. Existing surface measurements of methane do not have sufficient spatial coverage to adequately quantify the worldwide distribution of methane emissions. Thus, high-precision, spaceborne measurement techniques are necessary to obtain global coverage. Passive remote sensors such as SCIAMACHY [*Frankenberg et al.*, 2011], GOSAT [*Parker et al.*, 2011], CarbonSat [*Buchwitz et al.*, 2013], and Sentinel 5 [*Butz et al.*, 2012] measure the wavelength-resolved solar backscattered radiation from the surface of the Earth. However, these sensors are unable to measure at high latitudes during the winter months and their data are subject to bias in regions with aerosols layers or thin ice clouds [*Morino et al.*, 2011]. Spaceborne active remote sensing is thus a complementary approach because it can be more sensitive near the surface of the Earth, essentially has zero aerosol/cloud biases, and can measure during both daytime and nighttime. In order to realize this goal, Deusches Zentrum für Luft- und Raumfahrt (DLR) and Centre National d'Etudes Spatiales (CNES) proposed the "Methane Remote Sensing Lidar Mission" (MERLIN) in 2010 within the framework of a German-French climate-monitoring initiative [*Stephan et al.*, 2011]. This approach is based on the integrated-path differential-absorption (IPDA) LIDAR technique which measures the difference in atmospheric transmission between a laser emitting at a wavelength near the center of a methane absorption

feature [*Measures*, 1992], denoted online, and a reference off-line wavelength with no significant absorption [*Kiemle et al*., 2013, and references therein]. For MERLIN, the selected online wavelength is situated at the trough (λ = 1645.55 nm) between two strong absorption features which belong to the R(6) manifold of the $2\nu_3$ band of $^{12}CH_4$ [*Kiemle et al*., 2011]. By positioning the online wavelength in this local absorption minimum, the laser frequency stability requirement can be relaxed. The primary objective of the mission is to obtain spatial and temporal gradients of atmospheric methane columns with high precision and unprecedented accuracy on a global scale. Specifically, the mission targets for the measured methane columns are: 0.1% for systematic relative uncertainty (accuracy), and a statistical relative uncertainty (precision) of 1% at spatial and temporal resolutions of 50 km and 1 month, respectively [*Stephan et al*., 2011; *Kiemle et al*., 2013]. Therefore, the temperature-, pressure-, and wavelength-dependent absorption cross sections which describe the attenuation of the radiation by methane have to be known with extremely high accuracy in order to achieve this objective.

Many laboratory studies have been devoted to improving our spectroscopic knowledge of methane. The various spectroscopic parameters needed for calculating the absorption spectrum are line position, line-integrated intensity, and line shape (i.e., line width, line pressure-induced shift). From a remote sensing point of view, the absorption line shape parameter appears to be the most critical parameter. Inadequate modeling of the line shape, e.g., caused by erroneous spectroscopic broadening parameters or by the use of a deficient line shape model, typically results in gas concentration retrieval errors that exhibit latitudinal, seasonal, or other regionally varying biases. An overview of recent measurements of the line-shape parameters of the $2\nu_3$ band of $^{12}CH_4$ can be found in *Devi et al*. [2015]. The R(6) manifold was investigated by four studies, [*Frankenberg et al*., 2008; *Lyulin et al*., 2009; *Lyulin et al*., 2011; *Devi et al*., 2015], all of which were based on Fourier transform spectroscopy (FTS). Except for *Devi et al*. [2015], the other studies adopted the Voigt profile (VP) to represent the line shapes of isolated methane transitions. This profile is now considered as obsolete for many applications since it cannot reproduce absorption spectra to within a precision of a few percent [*Hartmann et al*., 2008; *Ngo et al*., 2013; *Birk and Wagner*, 2016]. Generally, other collisional (i.e., pressure-dependent) effects such as line mixing, Dicke narrowing, and speed dependence have to be taken into account in the line shape calculation in order to represent more accurately measured spectra. Furthermore, instrument-induced line shape distortion makes the precise determination of line shape parameters more challenging with traditional FTS methods. Also, the limited optical path length of the cells used in FTS spectrometers (leading to the need for samples with high absorber concentration) can render the contribution of methane self-broadening nonnegligible, which is a situation unfavorable for the precise determination of air-broadened line shapes.

The frequency-stabilized cavity ring-down spectroscopy (FS-CRDS) technique [*Hodges et al*., 2004; *Long et al*., 2012] offers a powerful alternative to traditional FTS methods, especially for precise measurements of optically thin spectra that are well below the detection limit of conventional spectrometers. In the FS-CRDS technique, absorption spectra are acquired by locking the probe laser frequency to successive modes of a length-stabilized, high-finesse optical resonator and by measuring the cavity decay rate associated with each mode. In this fashion, FS-CRDS spectra are obtained from measurements of time and frequency, resulting in accurate detuning (x) and absorption coefficient axes (y) and negligible instrumental line broadening. Importantly, this unique approach to CRDS provides the spectral resolution and linearity required for precise fits of non-Voigt line profiles and the concomitant determination of various line shape parameters [*Lisak et al*., 2010; *Long et al*., 2010; *Long et al*., 2011; *Lamouroux et al*., 2014; *Sironneau and Hodges*, 2015]. FS-CRDS typically yields spectrum signal-to-noise ratios in the 5×10^3:1 to 2×10^4:1 range, with some reported measurements ranging from 2×10^5:1 [*Cygan et al*., 2012] to 10^6:1 [*Lin et al*., 2015]. The accurate measurement of isolated transition areas on samples of known composition and density [*Sironneau and Hodges*, 2015; *Polyansky et al*., 2015] also yields low-uncertainty determinations (0.2% relative uncertainty level) of line intensities. With regard to measurements of transition frequencies and pressure-shifting coefficients, FS-CRDS can be referenced to highly accurate RF standards via an optical frequency comb (OFC) [*Truong et al*., 2013]. This scheme provides absolute transition frequencies (uncertainties from 10 kHz–100 kHz) as well as pressure shifting coefficients with relative uncertainties well below 1%.

In this work, an FS-CRDS apparatus [*Lin et al*., 2015] recently developed at the National Institute of Standard and Technology (NIST) in Gaithersburg, Maryland, USA, was used to record spectra of methane diluted in air. We measured spectra in the R(6) manifold region of the $2\nu_3$ band of $^{12}CH_4$ for six pressures in the range 40 hPa to 1013 hPa. These spectra were analyzed using multispectrum fitting of the model to the measured spectra, whereby the model parameters were adjusted simultaneously for all pressure conditions. The recently recommended line shape model, the Hartmann-Tran profile (HTP) [*Tennyson et al*., 2014; *Ngo*

et al., 2013], was used to calculate the isolated line shapes associated with the individual rotation-vibration transitions of the manifold. This profile takes into account Dicke narrowing, speed dependence effects and correlation between velocity-changing and internal-state-changing collisions. In addition, collisional interferences between lines (i.e., line mixing) were also accounted for by using the first-order approximation of Rosenkranz [*Ngo et al*., 2013; *Rosenkranz*, 1975].

In the remainder of this article we describe the FS-CRDS measurements of air-broadened methane and the associated multispectrum fitting results. Line parameters and their uncertainties for the investigated $^{12}CH_4$ transitions are reported. We also compare the present results to previous FTS measurements and existing spectroscopic line lists. Finally, using our measured methane line parameters and external database parameters for carbon dioxide and water vapor, we discuss calculated absorption spectra for an atmospheric column spanning the 4 cm^{-1} wide wave number region relevant to the MERLIN mission.

2. Experimental Apparatus

Here we provide only a brief overview of the FS-CRDS apparatus used in this work. For a more detailed description see *Lin et al.* [2015]. The sample cell comprises an all-stainless-steel vacuum-compatible enclosure (internal volume ≈ 250 cm^3) containing two high-finesse mirrors ($R = 0.99997$ at $\lambda = 1.65$ μm, radius of curvature = 1 m). The ring-down cavity length (≈138 cm) is actively stabilized by referencing to the simultaneous cavity transmission of an iodine-stabilized HeNe laser, which results in a long-term cavity mode frequency stability of approximately 10 kHz. The probe beam is provided by an external cavity diode laser followed by a booster-optical amplifier used for power amplification and rapid switching to initiate the ring-down decay events. At each spectrum step, the probe laser frequency is actively stabilized to a TEM_{00} mode of the ring-down cavity using a high-update-rate (400 Hz) wavelength meter with a frequency resolution of 1 MHz. At the beginning of each scan, the frequency axis is referenced to the heterodyne beat signal between the probe laser beam and a Cs clock-referenced optical frequency comb (OFC) having a fractional stability of 10^{-13} (1 s averaging time). Frequency detuning relative to the first point of the scan is determined by counting ring-down cavity mode orders as the laser is tuned from mode to mode of the ring-down cavity. The mode spacing or cavity free spectral range (FSR) is measured by step scanning the laser from mode to mode of the evacuated ring-down cavity and measuring the laser frequency at each step with a high-precision wavelength meter (resolution of 1 MHz), resulting in unc(FSR) = 2 kHz. At each pressure condition, we correct the empty-cavity FSR value for the effect of air density on optical pathlength using $dFSR/dp = -0.285$ Hz/Pa (based on the calculated dependence of air refractive index with density for a wavelength $\lambda = 1645.75$ nm and temperature $T = 23$°C). The combined standard uncertainty for the first point of the spectrum frequency axis is approximately 100 kHz and is limited by the precision of the laser frequency lock. There is a cumulative error along the detuning axis which is equal to $\Delta q \times$ u(FSR), where Δq is the number of mode jumps. For all spectra reported here $\Delta q < 500$, yielding a maximum uncertainty of about 1 MHz for the absolute frequency at all points. As previously described, [*Lin et al*., 2015], this spectrometer has a minimum detectable absorption coefficient of 1.5×10^{-12} cm^{-1} (10 s averaging time). In the present study, each spectral point is based on the average of 320 decay events, with successive spectrum points acquired every 7 s.

We acquired absorption spectra on static charges of the methane/air sample at temperatures near 296 K. We measured the gas pressure and temperature in the ring-down cell using NIST-calibrated pressure and temperature sensors having relative combined standard uncertainties generally less than 0.05% and 20 mK, respectively. The temperature sensor was in good thermal contact with the outside surface of the bounding stainless steel tube (1 m long, 2.5 cm diameter) containing the sample gas. We observed that the largest driver of temperature uncertainty was caused by axial gradients (maximum absolute difference <80 mK) in the cell wall temperature. Assuming ideal gas conditions and adding the pressure and temperature uncertainties in quadrature yields a relative combined standard uncertainty in sample gas density of 0.02%. In order to optimize the spectrum signal-to-noise ratio over the pressure range considered, we used a pair of high- (11.8736 μmol $mol^{-1} \pm 0.0039$ μmol mol^{-1}) and low- (1.192 μmol $mol^{-1} \pm 0.01$ μmol mol^{-1}) concentration mixtures of methane in air. Both mixtures were certified at NIST by reference to primary gravimetric standards. The specified concentrations correspond to total methane at natural isotopic abundance. For the spectrum model described below, we assumed the relative abundance of $^{12}CH_4$ in the total methane to be 0.98827. Tables 1a and 1b summarize the experimental conditions of the analyzed spectra, the corresponding standard uncertainties, and other experimental specifications.

Table 1a. Experimental Conditions for the Measured Spectra where P, T, and x are the Total Sample Pressure, Temperature, and Methane-In-Air Molar Fraction, respectively[a]

Spectrum	P (hPa)	unc(P)/P (%)	T (K)	unc(T)/T (%)	x (μmol mol^{-1})	unc(x)/x (%)	unc(n)/n (%)
1	40.535	0.046	296.225	0.025	11.8736	0.033	0.062
2	133.64	0.028	296.183	0.027	11.8736	0.033	0.051
3	402.89	0.025	296.097	0.028	11.8736	0.033	0.050
4	506.49	0.019	296.129	0.030	11.8736	0.033	0.048
5	760.69	0.014	296.110	0.028	1.192	0.839	0.839
6	1013.53	0.013	296.106	0.029	1.192	0.839	0.840

[a]For each quantity, uncertainty components are added in quadrature. In the case of pressure and temperature, the component uncertainties include the standard deviation of the respective measurements for each spectrum and the combined standard uncertainty in the pressure or temperature gauge. The temperature uncertainty also includes a component associated with temperature gradients in the sample gas. The final column gives the relative combined standard uncertainty for the total methane concentration n, which is assumed to be at natural isotopic abundance.

3. Spectrum Analysis

The measured spectra were analyzed using a multispectrum fitting technique [*Benner et al.*, 1995] in which all six measured spectra (Tables 1a and 1b) were fitted by simultaneous adjustment of the model parameters. This technique allows one to constrain the linear pressure dependence of line shape parameters and to decrease the numerical correlation between these parameters. The fitting procedure was realized using a code that we recently developed and which provides adjustable parameters related to each spectrum considered and to each spectral line. A particular feature of this code is that we can calculate complex line profiles, such as the HTP [*Ngo et al.*, 2013; *Tennyson et al.*, 2014], along with line mixing through the first-order approximation of Rosenkranz [*Rosenkranz*, 1975]. Moreover, because methane molar fractions for all measured spectra did not exceed 12 μmol mol^{-1}, we were able to safely neglect the effects of methane self-broadening. Only parameters of the six R(6) manifold lines of $^{12}CH_4$ were adjusted during the fitting process. Contributions of weak interfering lines having intensities lower than 1.0×10^{-23} cm/molecule at temperature $T=296$ K were calculated using the HITRAN 2012 [*Rothman et al.*, 2013; *Brown et al.*, 2013; *Campargue et al.*, 2013] line parameters and then fixed. Figure 1 shows that the contribution of weak lines in the considered spectral range is satisfactorily reproduced using line parameter data from the 2012 version of the HITRAN database [*Rothman et al.*, 2013].

Using the HTP to represent the line shape and taking into account the line-mixing effect, the absorption coefficient versus wavenumber σ (cm^{-1}) is calculated through [*Ngo et al.*, 2013]

$$\alpha(\sigma)=\sum_l \frac{S_l n_{CH_4}}{\pi}\left[\mathrm{Re}\left\{I_l^{HTP}(\sigma)\right\}-Y_l\,\mathrm{Im}\left\{I_l^{HTP}(\sigma)\right\}\right]. \quad (1)$$

The sum in equation (1) is over the six lines of the R(6) manifold, $Y_l=P\zeta_l$ is the first-order line-mixing parameter, representing the coupling between the line l and other lines. S_l and n_{CH_4} are the line-integrated intensity (at natural isotopic abundance) and the number density of total methane, respectively. Using the ideal gas law and the known molar fraction of methane, x_{CH_4}, we calculate $n_{CH_4}=x_{CH_4}P/(k_BT)$ where P and T are the total gas pressure and temperature, respectively, and k_B is the Boltzmann constant.

Within the HTP model, the $I_l^{HTP}(\sigma)$ line shape quantity is a function of eight parameters [*Ngo et al.*, 2013], i.e.,

$$I_{HTP}(\sigma)=f(\sigma-\sigma_0,\Gamma_D,\Gamma_0,\Gamma_2,\Delta_0,\Delta_2,\nu_{VC},\eta), \quad (2)$$

with σ_0 representing the unperturbed position of the line. The HTP model takes into account the main processes affecting the shape of an isolated line in the binary-collision regime. These include the following four effects. (1) Doppler broadening (through the Doppler broadening halfwidth Γ_D); (2) velocity-changing collisions (Dicke narrowing) induced by intermolecular collisions, which is described through the hard-

Table 1b. Experimental Specifications for Ring-Down Apparatus

System Parameters	Values
Ring-down cavity length[a] (cm)	137.84
Empty-cavity FSR[a] (MHz)	108.75
unc(FSR) (kHz)	2
unc(ν) (MHz)	1
Mirror reflectivity[a]	0.99997
Number of ring-down acquisitions per frequency step	320

[a]Denotes a nominal value.

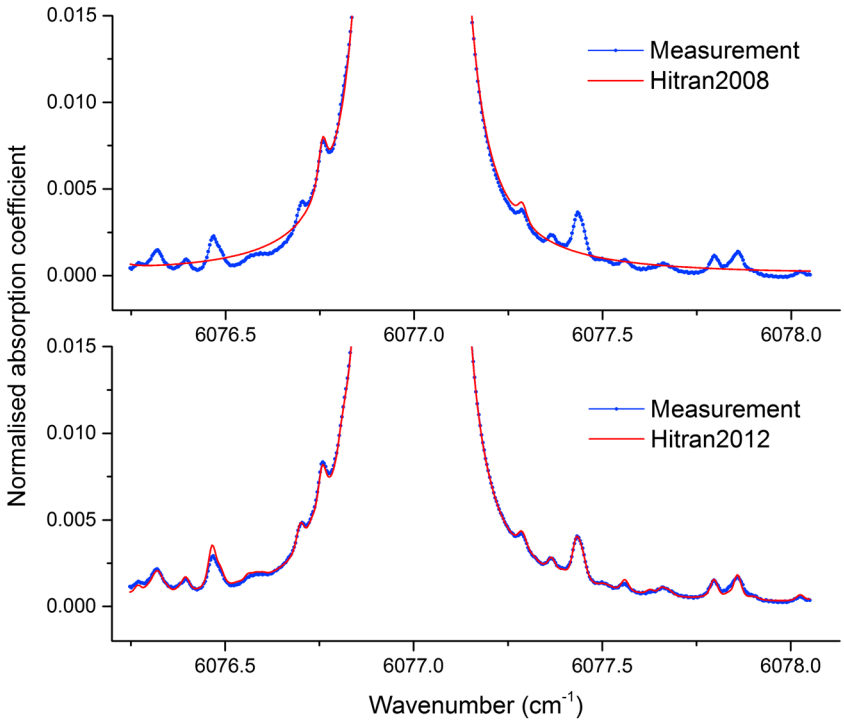

Figure 1. Comparison between the present FS-CRDS-measured spectra and HITRAN-calculated values for air-broadened methane at room temperature and $P = 133$ hPa. (top) HITRAN 2008 [*Rothman et al*., 2009]; (bottom) HITRAN 2012 [*Rothman et al*., 2013].

collision model [*Nelkin and Ghatak*, 1964; *Rautian and Sobel'man*, 1967] and parameterized in terms of the rate of velocity-changing collisions ν_{vc} (or the Dicke narrowing frequency); (3) speed dependences of the collisional halfwidth $\Gamma(\nu)$ and shift $\Delta(\nu)$ modeled by the quadratic law and first proposed by *Rohart et al*. [1994] and *Rohart et al*. [1997] $\Gamma(\nu) + i\Delta(\nu) = \Gamma_0 + i\Delta_0 + (\Gamma_2 + i\Delta_2)[(\nu/\tilde{\nu})^2 - 3/2]$ where $\tilde{\nu} = \sqrt{2k_B T/m}$ is the most probable speed for an absorbing molecule of mass m; and (4) temporal correlation between velocity-changing and internal-state-changing collisions, which is accounted for through the correlation parameter η. The line parameters of the HTP vary simply with the total pressure P: σ_0, and η are constant while ν_{vc}, Γ_0, Γ_2, Δ_0, and Δ_2 are proportional to P. Note that from equation (2) the majority of models used to describe measured absorption spectra [*Ngo et al*., 2013, and references therein] can be directly obtained as limits of the HTP, by fixing appropriate parameters to zero.

In our fitting procedure, for each line, the shared parameters (i.e., common parameters for all considered pressures) are then $\frac{\Gamma_0}{P}, \frac{\Gamma_2}{P}, \frac{\Delta_0}{P}, \frac{\Delta_2}{P}, \frac{\nu_{vc}}{P}$, η, and $\frac{Y}{P}$, together with the zero-pressure position of the line σ_0 and the relative integrated line intensity, i.e., S_i/S_{tot} with S_{tot} the spectrum area. Note that the Dicke narrowing parameter $\frac{\nu_{vc}}{P}$ was fitted but imposed to be the same for all six transitions during the fitting procedure. Finally, for each spectrum, a linear base line with two adjustable parameters, representing the zero absorption level, and the total area were also retrieved. Note that the Doppler contribution is calculated from the considered temperature for each transition and then fixed. In total, $(49 + 3 \times 6$ spectra) parameters were adjusted for the six transitions with a total of six measured spectra. Because the CH_4 concentrations of the first four spectra (see Table 1a) in the mixtures were known with a very high precision, these spectra were used to deduce absolute intensity for the six considered transitions.

4. Results

4.1. Fit Residuals and Obtained Parameters

As shown in Figure 2, the considered $2\nu_3$ R(6) manifold is formed by two distinct groups of three transitions each, which remain almost unresolved even at low pressure. It is thus particularly challenging to correctly

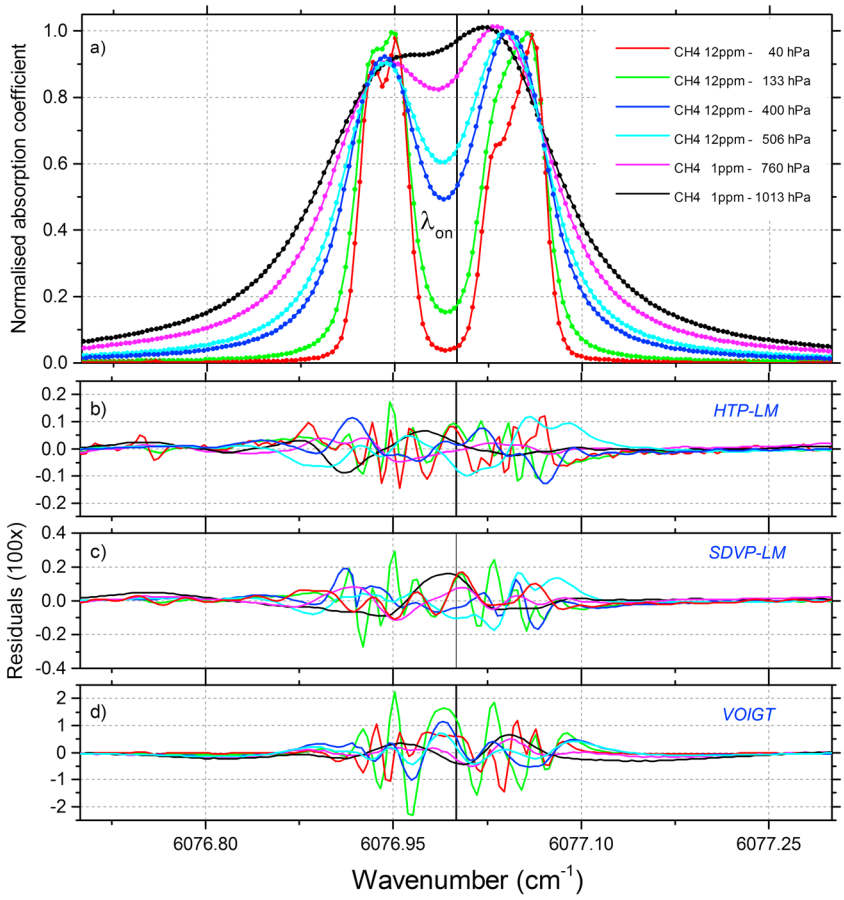

Figure 2. Multispectrum fit results of the six air-broadened spectra in the $2\nu_3$ R(6) $^{12}CH_4$ manifold region. (a) All the spectra (normalized to their peak absorption) considered: measurements are represented using dots while lines are for the modeled absorptions. (b) The fit residuals (observed minus calculated) using the first-order line-mixing HTP (expanded scale × 100); (c) those obtained using the first-order line-mixing speed-dependent Voigt profile; (d) the fit residuals obtained with the VP. The wavenumber position of the MERLIN online is also indicated as a thick black line.

retrieve parameters for each line of the manifold. The initial $2\nu_3$ R(6) parameters are set as follows: line positions $\sigma_{0,I}$ and line intensities were taken from HITRAN 2012, line-broadening and line-shifting coefficients, $\Gamma_{0,I}/P$ and $\Delta_{0,I}/P$, were based on those of the ν_3 manifold [*Pine*, 1997] as done in *Tran et al.* [2010], and the first-order line-mixing parameters ζ_I, were calculated from the relaxation matrix elements of *Tran et al.* [2010, 2006].

The multispectrum fit of the $2\nu_3$ R(6) $^{12}CH_4$ manifold, extending from 6076.7 to 6077.3 cm^{-1} is shown in Figure 2a, along with the fit residuals (Figure 2b) for the six considered spectra. The results obtained with the same measured spectra but by using the commonly used VP (no line mixing nor Dicke narrowing and speed dependence) and with the speed-dependent Voigt profile combined with the first-order line mixing are also reported for comparison (Figures 2c and 2d). As can be observed, the VP leads to large deviations with respect to the measured spectra, with differences of up to ±2% (Figure 2d). When line-mixing and speed dependence effects are taken into account (Figure 2c), the fit residuals are of about ±0.2%. Finally, when the HTP (Figure 2b) is used together with the first-order line mixing, excellent agreement is obtained with a maximum residual deviation of ±0.12% for all considered pressures. Particularly, the fit residuals are always lower than 0.1% around the MERLIN online wave number near $\sigma = 6077\ cm^{-1}$. This is the first time that such an accuracy is reached in the modeling of the $2\nu_3$ R(6) $^{12}CH_4$ manifold, completely fulfilling the accuracy requirements for MERLIN [*Kiemle et al.*, 2011; *Kiemle et al.*, 2013; *Stephan et al.*, 2011]. Note that sources of uncertainty associated with the measured spectra should not be critical here because of the high signal-to-noise ratio (>20,000:1), the small relative combined uncertainty of the pressure and temperature measurements

Table 2. Measured Line Parameters for the R(6) Manifold in the $2\nu_3$ Band of $^{12}CH_4$[a]

R6 Transition	Fitted Position (cm^{-1})	Intensity (cm/molecule)	Γ_0/P (10^{-3} cm^{-1}/atm)	Δ_0/P (10^{-3} cm^{-1}/atm)	ζ_1/P (10^{-1} cm^{-1}/atm)	ν_{VC}/P (10^{-3} cm^{-1}/atm)	Γ_2/P (10^{-3} cm^{-1}/atm)	Δ_2/P (10^{-3} cm^{-1}/atm)	η
7E ← 6E 1	6076.92716(9)	$4.52(6)\cdot10^{-22}$	66.75(71)	−25.65(66)	-	19.36(99)	24.95(83)	−1.97(72)	0.540(24)
7 F1 ← 6 F2 1	6076.93411(9)	$7.91(7)\cdot10^{-22}$	53.16(40)	−3.43(41)	−3.9(26)		3.08(45)	12.85(35)	0.273(22)
7A1 ← 6A2 1	6076.95316(1)	$1.22(1)\cdot10^{-21}$	65.29(14)	−9.48(12)	−0.96(16)		13.49(21)	−3.27(17)	0.239(18)
7 F1 ← 6 F2 2	6077.02785(1)	$7.29(6)\cdot10^{-22}$	54.35(26)	−6.15(32)	3.89(25)		0.0[b]	−5.63(23)	0.123(21)
7 F2 ← 6 F1 1	6077.04639(2)	$7.35(7)\cdot10^{-22}$	43.68(16)	−13.79(31)	2.31(15)		3.54(34)	−5.30(26)	0.614(33)
7A2 ← 6A1 1	6077.06296(1)	$1.20(1)\cdot10^{-21}$	60.45(16)	−9.05(16)	−0.24(8)		11.39(19)	−1.37(21)	0.257(16)

[a]The uncertainties in parentheses are 1 sigma internal statistical errors in the last quoted digit(s); as an example, 6076.92716(9) cm^{-1} means 6076.92716(0.00009) cm^{-1}. Values can be converted to SI units using the factor 1 cm^{-1} atm^{-1} = 0.295872 MHz Pa^{-1}.
[b]Ill-defined parameter, set to 0.

(around 0.03%) and the accuracy of absolute and relative frequency scales (standard uncertainty of nominally 1 MHz ≈ 3.3×10^{-5} cm^{-1}) of the FS-CRDS experiment.

The retrieved spectroscopic parameters for the $2\nu_3$ R(6) $^{12}CH_4$ manifold are listed in Table 2 together with their associated standard deviations (1 σ statistical errors reported by the fitting program). The illustrated variation in the intensity ratios from the expected 5:3:2 values can be interpreted as perturbations between nearby levels. Nonetheless, it is apparent that these parameters remain close to their initial values derived from to "HITRAN 2012 [*Rothman et al.*, 2013], resulting in a fine tuning of the initial parameters. With regard to other parameters, the direct comparison with previous studies is difficult because of differences in the line shape models considered. We noticed for example that our values of the broadening parameters $\frac{\Gamma_0}{P}$ were slightly lower than those of other studies [*Pine*, 1997; *Devi et al.*, 2015]. Due to the strong overlapping within the considered R(6) transitions, the first-order approximation is not able to fully describe line mixing, thus leading to effective line-mixing parameters which do not satisfy the sum rule [*Hartmann et al.*, 2008]. Nevertheless, our set of parameters together with our line shape model provide the best available modeling of the absorption in the R(6) manifold of the $2\nu_3$ band of $^{12}CH_4$. A meaningful way to test the ascribed accuracy is to compute the residuals obtained

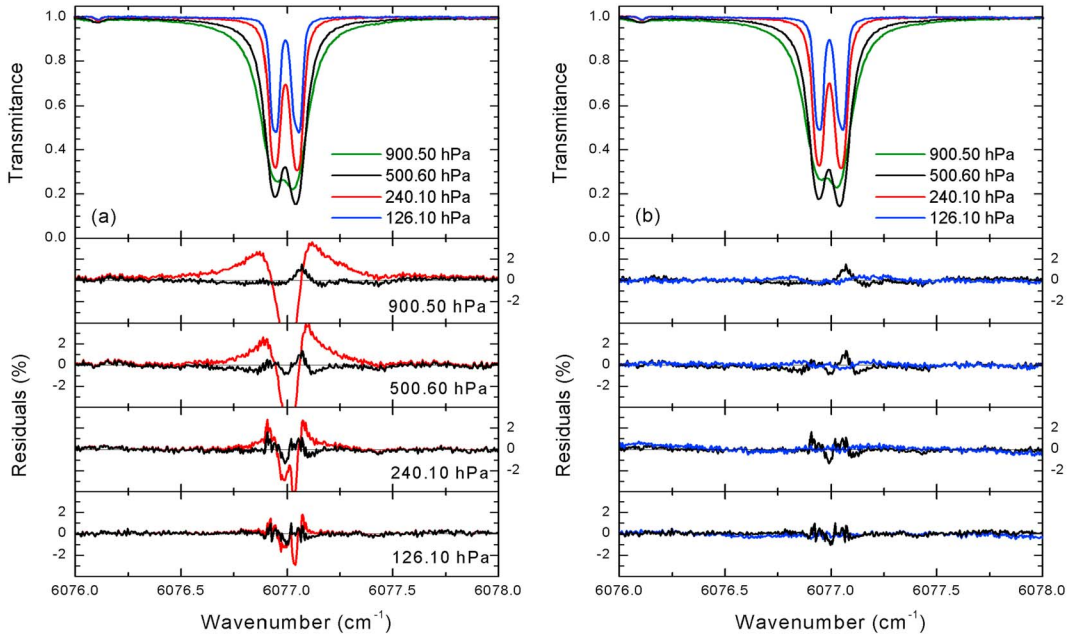

Figure 3. (a, b) Transmittance spectra measured by an FTS spectrometer (Set 1) [*Frankenberg et al.*, 2008] (first panels) and differences (second to fifth panels) between these measurements and calculated spectra. Black and red residuals correspond to a model based on positions and intensities from HITRAN 2008 and line-broadening and line-shifting coefficients estimated from the data of *Pine* [1997], with (black) and without (red) line mixing taken into account. Blue residuals correspond to the present model (obtained from fits to the FS-CRDS data).

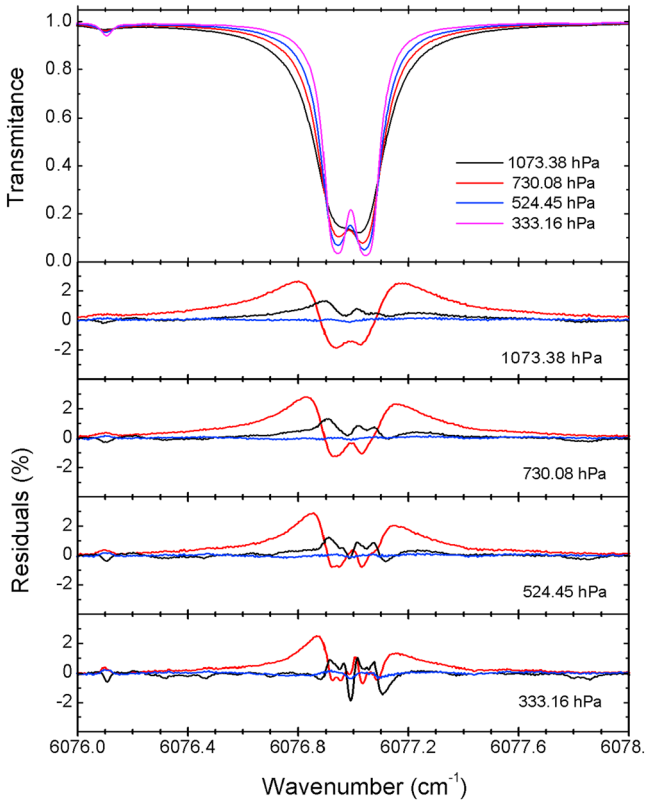

Figure 4. (first panel) Transmittances measured by an FTS spectrometer (Set 2, [*Devi et al*., 2015]) and (second to fifth panels) differences between these measurements and calculated spectra. Calculations are based on first-order line-mixing with the HTP (present case, blue lines), VP with HITRAN 2012 line parameters (red lines, [*Rothman et al*., 2013]), and VP with HITRAN 2008 (black lines, [*Rothman et al*., 2009]).

through comparisons of modeled spectra (based on the present HTP-line-mixing fits) with previous high-precision measurements.

4.2. Intercomparisons With FTS Measurements

In order to test the model for the wavenumber region presented above, we compared the resulting predictions with spectra measured by other groups. We note that these previous data were based on different experimental techniques and corresponded to other pressure conditions. Specifically, we used two sets of measured spectra of *Frankenberg et al*. [2008] and *Devi et al*. [2015]. For the first set (Set 1), four spectra of methane diluted in N_2 were measured at room temperature for pressures ranging from 126 hPa to 900 hPa using a high-resolution FTS spectrometer [*Frankenberg et al*., 2008]. In the second set (Set 2), four air-broadened, room temperature methane FTS spectra of *Devi et al*. [2015] were measured at pressures from 331 hPa to 1179 hPa. Details of the experimental setups and conditions can be found in the corresponding references.

From the spectroscopic parameters obtained in this work (see Table 2), synthetic spectra were calculated for exactly the same temperature and pressure conditions as those of the previous measurements. The contribution of methane self-broadening to the spectra is not negligible in these prior cases (i.e., the relative partial pressure of CH_4 of Set 1 was about 1–2% while it was about 0.3–1% for Set 2) and therefore was taken into account. The contributions of self-broadening, and line-mixing coefficients for pure methane were taken from the values of *Devi et al*. [2015] and estimated as discussed by *Tran et al*. [2015]. The instrument line shape functions of the two FTS spectrometers were also accounted for by using data provided by the authors of *Frankenberg et al*. [2008] and *Devi et al*. [2015] and by using the LINEFIT software developed by F. Hase [*Hase et al*., 1999]. Finally, except for a scaling factor for the spectrum area, the calculated spectra were directly compared with measured transmittances without using any adjustable parameters.

Figure 3 presents the comparison between the measured spectra of Set 1 and those calculated using the different spectroscopic line parameter data sets. Line shape parameters for N_2-broadened methane were obtained from those of air-broadened methane using the corresponding ratios of *Pine and Gabard* [2003]. In Figure 3a, spectra were calculated using line positions and intensities provided in HITRAN 2008 [*Rothman et al*., 2009] and line-broadening and line-shifting coefficients estimated from data of *Pine* [1997]. The latter were obtained from high-quality measurements in the ν_3 band of methane. In Figure 3a, residuals obtained for the four considered pressures with line mixing (black lines) and without line mixing (red lines) taken into account are plotted. These results illustrate the importance of the line-mixing contribution to the shape of methane spectra. In Figure 3b, measured spectra are compared with those calculated using the spectroscopic line parameters

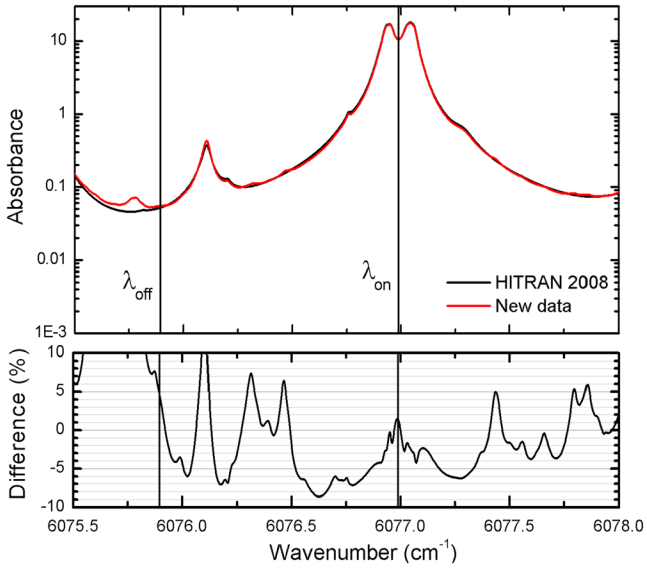

Figure 5. (top) Comparison of the total column-integrated absorption spectra (including CH_4, H_2O, and CO_2 absorption) derived using HITRAN 2008 parameters (black) and our new model for the R(6) manifold along with HITRAN 2012 parameters for other weak lines (red). (bottom) Relative difference between the two spectra, in percent. Meteorological data were obtained from the U. S. standard model. Vertical lines mark off-line and online MERLIN instrument operating wavelengths, respectively.

spectroscopic line parameters obtained in the present work, using the HTP and taking line mixing into account. The corresponding residuals are plotted in blue. The black residuals of Figure 3a are also plotted in Figure 3b for comparison. As can be observed, the new spectroscopic parameters, used together with our code lead to very good agreement with measured spectra, much better than with previous line parameter data, with the obtained residuals being almost within the experimental noise level.

The comparison between the air-broadened methane measured spectra of Set 2 [*Devi et al*., 2015] and calculated transmittances is presented in Figure 4. Residuals between measurements and spectra calculated using spectroscopic parameters obtained in this work and the associated spectral profiles (first-order line-mixing HTP) are plotted in blue in the second to fifth panels. Recall that calculations were done for exactly the same pressure and temperature conditions as those of the measurements and no adjustable parameters were used for these comparisons. In order to compare our results with the different existing spectroscopic data sources, calculations were also performed using spectroscopic parameters of the 2008 [*Rothman et al*., 2009] and the 2012 [*Rothman et al*., 2013] versions of the HITRAN database. The corresponding residuals for all considered pressures are plotted in black and red lines, respectively. Surprisingly, the spectroscopic data set of HITRAN 2008 lead to much better agreement with measured spectra than those of HITRAN 2012. This is probably a result of the inconsistency between the line-broadening coefficients provided in HITRAN 2012 for these lines and the use of the VP. As can be observed in Figure 4, our new data lead to much better agreement with measured spectra. Differences between all measured spectra and our calculations are almost always better than about 0.2%, except for the case of the lowest pressure (i.e., Figure 4, fifth panel) where a slightly larger set of residuals is obtained. The latter is probably caused by uncertainty in the assumed FTS instrument line shape function, determined from low-pressure HCl spectra which were recorded simultaneously with air-broadened methane spectra [*Devi et al*., 2015].

5. Discussion and Conclusions

Absorption of methane in the 1.64 μm region was precisely measured using a frequency-stabilized cavity ring-down spectroscopy spectrometer at room temperature and various pressures. These spectra were analyzed using the latest standard line shape profile which takes into account line-mixing, Dicke narrowing, and speed dependence effects. The obtained data and model enable calculation of synthetic spectra to within 0.12% of measurements and yield even better agreement at the online position of the MERLIN mission. Using the spectroscopic data derived from implementing the commonly used Voigt profile led to deviations of up to 2% between the calculated and measured absorption coefficients. Note that for MERLIN and atmospheric applications in general, data at lower temperature are also required. To address this need, we will make high-sensitivity CRDS measurements with a new variable-temperature apparatus. The same line shape model will be used for spectrum analysis. In particular, we will quantify the temperature dependence of the non-Voigt line shape parameters over the atmospheric temperature range. These studies will be presented in a forthcoming paper. The other issue concerning the spectroscopy for MERLIN is the broadening of methane lines by water vapor. In order to quantify the magnitude of this effect, a study has been performed by our

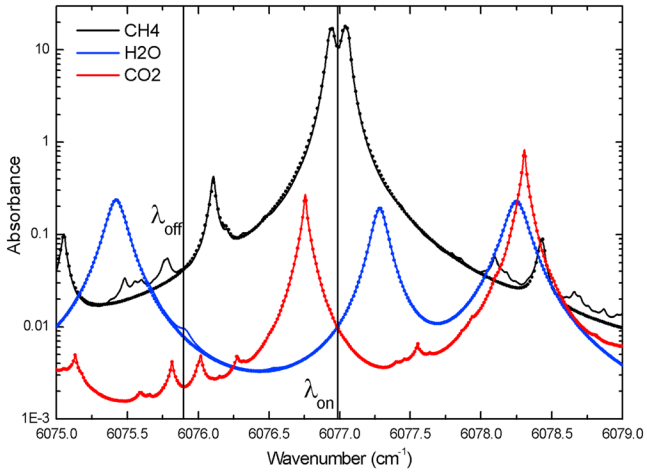

Figure 6. Comparisons of the CH_4, CO_2, and H_2O total column-integrated absorption spectra calculated using spectroscopic data of HITRAN 2008 (dots) and our data for the $2\nu_3$ R(6) manifold of $^{12}CH_4$ together with HITRAN 2012 for other lines and species (lines).

group showing that broadening of methane lines by water vapor is about 30% more efficient than that of dry air [*Delahaye et al*., 2016].

In order to quantify the influence of these new spectroscopic data and model for atmospheric observations, we carried out simple radiative transfer calculations assuming the U.S. standard atmospheric condition model. The results are shown in Figure 5 in which atmospheric spectra (including absorption by methane, water vapor, and carbon dioxide) calculated by using HITRAN 2008 parameters (black) and our new model for the R(6) manifold along with HITRAN 2012 parameters for other lines (red) are plotted. The relative difference observed between the two spectra, plotted in Figure 5 (bottom), is of the order of 5% and 1.5% in the off-line and online MERLIN spectral regions, respectively. The latter is consistent with residuals observed using VP to describe absorption by $^{12}CH_4$ in the R(6) manifold (Figure 2c). This again emphasizes the importance of properly modeling the line shape and choice of spectroscopic parameters for precise remote sensing atmospheric applications. For the off-line region (6075.896 cm^{-1}), analyzing the contribution of each species (Figure 6) shows that there are significant differences between absorbances calculated using HITRAN 2008 and HITRAN 2012 for methane and water vapor. As already shown in Figure 1, spectroscopic data in HITRAN 2012 for $^{12}CH_4$ in this 1.64 μm region are much more complete than in HITRAN 2008. Similarly, several weak lines of H_2O were also added in the 2012 version of the database. Hence, these lines must be taken into account in any performance calculation for MERLIN.

Acknowledgments

The authors would like to thanks B. Millet, C. Pierangelo, and J. M. Hartmann for helpful discussions. The research is partially supported by the French Space Agency, Centre National d'Etudes Spatiales. B. Drouin and C. Benner are acknowledged for helpful discussions about spectra intercomparison. S.E. Maxwell, Z.D. Reed, and J.T. Hodges were supported by the Greenhouse Gas and Climate Sciences Measurement Program of the National Institute of Standards and Technology. The research at the College of William and Mary and at the Jet Propulsion Laboratory, California Institute of Technology was performed under contracts and cooperative agreements with the National Aeronautics and Space Administration. The recorded laboratory spectra are available upon request to the corresponding author (ha.tran@lisa.u-pec.fr).

References

Benner, D. C., C. P. Rinsland, V. M. Devi, M. A. H. Smith, and D. Atkins (1995), A multispectrum nonlinear least squares fitting technique, *J. Quant. Spectrosc. Radiat. Transfer*, *53*, 705–721.

Birk, M., and G. Wagner (2016), Voigt profile introduces optical depth dependent systematic errors—Detected in high resolution laboratory spectra of water, *J. Quant. Spectrosc. Radiat. Transfer*, *170*, 159–168.

Brown, L. R., et al (2013), Methane line parameters in the HITRAN2012 database, *J. Quant. Spectrosc. Radiat. Transfer*, *130*, 201–219.

Buchwitz, M., et al. (2013), Carbon monitoring satellite (CarbonSat): Assessment of atmospheric CO_2 and CH_4 retrieval errors by error parameterization, *Atmos. Meas. Tech.*, *6*, 3477–3500, doi:10.5194/amt-6-3477-2013.

Butz, A., A. Galli, O. Hasekamp, J. Landgraf, P. Tol, and I. Aben (2012), I: TROPOMI aboard Sentinel-5 precursor: Prospective performance of CH_4 retrieval for aerosol and cirrus loaded atmospheres, *Remote Sens. Environ.*, *120*, 267–276, doi:10.1016/j.rse.2011.05.030.

Campargue, A., O. Leshchishina, L. Wang, D. Mondelain, and S. Kassi (2013), The WKLMC empirical line lists (5852–7919 cm^{-1}) for methane between 80 K and 296 K: "Final" lists for atmospheric and planetary applications, *J. Mol. Spectrosc.*, *291*, 16–22.

Cygan, A., D. Lisak, S. Wójtewicz, J. Domysławska, J. T. Hodges, R. S. Trawiński, and R. Ciuryło (2012), High-signal-to-noise ratio laser technique for accurate measurements of spectral line parameters, *Phys. Rev. A*, *85* 022508.

Delahaye, T., X. Landsheere, E. Pangui, F. Huet, J.-M. Hartmann, and H. Tran (2016), Measurements of H_2O broadening coefficients of infrared methane lines, *J. Quant. Spectrosc. Radiat. Transfer*, *173*, 40–48.

Devi, V. M., D. C. Benner, K. Sung, T. J. Crawford, S. Yu, L. R. Brown, M. A. H. Smith, A. W. Mantz, V. Boudon, and S. Ismail (2015), Self-and air-broadened line shapes in the $2\nu_3$ P and R branches of $^{12}CH_4$, *J. Mol. Spectrosc.*, *315*, 114–136.

Frankenberg, C., T. Warneke, A. Butz, I. Aben, F. Hase, P. Spietz, and L. B. Brown (2008), Pressure broadening in the $2\nu_3$ band of methane and its implication on atmospheric retrievals, *Atmos. Chem. Phys.*, *8*, 5061–5075.

Frankenberg, C., I. Aben, P. Bergamaschi, E. J. Dlugokenckv, R. van Hees, S. Houweling, P. van der Meer, R. Snel, and P. Tol (2011), Global column averaged methane mixing ratios from 2003 to 2009 as derived from SCIAMACHY: Trends and variability, *J. Geophys. Res.*, *116*, D04302, doi:10.1029/2010JD014849.

Hartmann, J.-M., C. Boulet, and D. Robert (2008), *Collisional Effects on Molecular Spectra. Laboratory Experiments and Model, Consequences for Applications*, Elsevier, Amsterdam.

Hase, F., T. Blumenstock, and C. Paton-Walsh (1999), Analysis of the instrumental line shape of high-resolution Fourier transform IR spectrometers with gas cell measurements and new retrieval software, *Appl. Opt.*, *38*, 3417–22.

Hodges, J. T., H. P. Layer, W. W. Miller, and G. E. Scace (2004), Frequency-stabilized single- mode cavity ring-down apparatus for high-resolution absorption spectroscopy, *Rev. Sci. Instrum.*, *75*, 849–863.

Kiemle, C., M. Quatrevalet, G. Ehret, A. Amediek, A. Fix, and M. Wirth (2011), Sensitivity studies for a spaced-based methane lidar mission, *Atmos. Meas. Tech.*, *4*, 2195–2211, doi:10.5194/amt-4-2195-2011.

Kiemle, C., S. R. Kawa, M. Quatrevalet, and E. V. Browell (2013), Performance simulations for a spaceborne methane lidar mission, *J. Geophys. Res. Atmos.*, *119*, 4365–4379, doi:10.1002/2013JD021253.

Kirschke, S., et al (2013), Three decades of global methane sources and sinks, *Nat. Geosci.*, *6*, 813–823.

Lamouroux, J., V. Sironneau, J. T. Hodges, and J.-M. Hartmann (2014), Isolated line shapes of molecular oxygen: Requantized classical molecular dynamics calculations versus measurements, *Phys. Rev. A*, *89* 042504.

Lin, H., Z. D. Reed, V. T. Sironneau, and J. T. Hodges (2015), Cavity ring-down spectrometer for high-fidelity molecular absorption measurements, *J. Quant. Spectros. Radiat. Transfer*, *161*, 11–20.

Lisak, D., P. Masłowski, A. Cygan, K. Bielska, S. Wójtewicz, M. Piwiński, J. T. Hodges, R. S. Trawiński, and R. Ciuryło (2010), Line shapes and intensities of self-broadened O_2 b1Sg + (n = 1) – X3Sg- (n = 0) band transitions measured by cavity ring-down spectroscopy, *Phys. Rev. A*, *81*, 042504.

Long, D. A., D. K. Havey, M. Okumura, C. E. Miller, and J. T. Hodges (2010), O_2 A-band line parameters to support atmospheric remote sensing, *J. Quant. Spectros. Radiat. Transfer*, *111*, 2021–2036.

Long, D. A., K. Bielska, D. Lisak, D. K. Havey, M. Okumura, C. E. Miller, and J. T. Hodges (2011), The air-broadened, near-infrared CO_2 line shape in the spectrally isolated regime: Evidence of simultaneous Dicke narrowing and speed dependence, *J. Chem. Phys.*, *135* 064308.

Long, D. A., A. Cygan, R. D. van Zee, M. Okumura, C. E. Miller, and J. T. Hodges (2012), Frequency-stabilized cavity ring-down spectroscopy, *Chem. Phys. Lett.*, *536*, 1–8.

Lyulin, O. M., A. V. Nikitin, V. I. Perevalov, I. Morino, T. Yokota, R. Kumazawa, and T. Watanabe (2009), Measurements of N_2- and O_2-broadening and shifting parameters of methane spectral lines in the 5550–6236 cm^{-1} region, *J. Quant. Spectrosc. Radiat. Transfer*, *110*, 654–668.

Lyulin, O. M., V. I. Perevalov, I. Morino, T. Yokota, R. Kumazawa, and T. Watanabe (2011), Measurement of self-broadening and self-pressure-induced shift parameters of the methane spectral lines in the 5556–6166 cm^{-1} range, *J. Quant. Spectrosc. Radiat. Transfer*, *112*, 531–539.

Measures, R. M. (1992), *Laser Remote Sensing: Fundamentals and Applications*, Krieger Publishing Company, Malabar, Fla.

Morino, I., et al (2011), Preliminary validation of column-averaged volume mixing ratio of carbon dioxide and methane retrieved from GOSAT short-wavelength infrared spectra, *Atmos. Meas. Tech.*, *4*, 1061–1076, doi:10.5194/amt-4-1061-2011.

Nelkin, M., and A. Ghatak (1964), Simple binary collision model for Van Hove's G_s(r,t), *Phys. Rev.*, *135*, A4–A9.

Ngo, N. H., D. Lisak, H. Tran, and J.-M. Hartmann (2013), An isolated line shape model to go beyond the Voigt profile in spectroscopic databases and radiative transfer codes, *J. Quant. Spectrosc. Radiat. Transfer*, *129*, 89–100.

Parker, R., et al. (2011), Methane observations from the Greenhouse Gases Observing SATellite: Comparison to ground based TCCON data and model calculations, *Geophys. Res. Lett.*, *38*, L15807, doi:10.1029/2011GL047871.

Pine, A. S. (1997), N_2 and Ar broadening and line mixing in the P and R branches of the ν_3 band of CH_4, *J. Quant. Spectrosc. Radiat. Transfer*, *57*, 157–176.

Pine, A. S., and T. Gabard (2003), Multispectrum fits for line mixing in the ν_3 band Q branch of methane, *J. Mol. Spectrosc.*, *217*, 105–114.

Polyansky, O. L., K. Bielska, M. Ghysels, L. Lodi, N. F. Zobov, J. T. Hodges, and J. Tennyson (2015), High-accuracy CO_2 line intensities determined from theory and experiment, *Phys. Rev. Lett.*, *114* 243001.

Rautian, S. G., and I. I. Sobel'man (1967), The effect of collisions on the Doppler broadening of spectral lines, *Sov Phys.-Usp.*, *9*, 701–716.

Rohart, F., H. Mader, and H. W. Nicolaisen (1994), Speed dependence of rotational relaxation induced by foreign gas collisions: Studies on CH_3F by millimeter wave coherent transients, *J. Chem. Phys.*, *101*, 6475–6486.

Rohart, F., A. Ellendt, F. Kaghat, and H. Mäder (1997), Self and polar foreign gas line broadening and frequency shifting of CH_3F: Effect of the speed dependence observed by millimeter-wave coherent transients, *J. Mol. Spectrosc.*, *185*, 222–233.

Rosenkranz, P. K. (1975), Shape of the 5 mm oxygen band in the atmosphere, *IEEE Trans. Antennas Propag.*, *23*, 498–506.

Rothman, L. S., et al (2009), The HITRAN 2008 molecular spectroscopic database, *J. Quant. Spectros. Radiat. Transfer*, *10*, 533–72.

Rothman, L. S., et al (2013), The HITRAN 2012 molecular spectroscopic database, *J. Quant. Spectrosc. Radiat. Transfer*, *130*, 4–50.

Stephan, C., M. Alpers, B. Millet, G. Ehret, P. Flamant, and C. Deniel (2011), MERLIN: A space-based methane monitor, in *Proc. SPIE, Opt. Photonics Conf.*, vol. 8159, pp. 815–908, Lidar Remote Sensing for Environmental Monitoring XII, San Diego, Calif.

Sironneau, V. T., and J. T. Hodges (2015), Line shapes, positions and intensities of water transitions near 1.28 μm, J. Quant. Spectros. Radiat. *Transfer*, *152*, 1-15.

Tennyson, J., et al. (2014), Recommended isolated-line profile representing high-resolution spectroscopic transitions, *Pure Appl. Chem.*, *86*, 1931–43.

Tran, H., P.-M. Flaud, T. Gabard, F. Hase, T. von Clarmann, C. Camy-Peyret, S. Payan, and J.- M. Hartmann (2006), Model, software and database for line-mixing effects in the ν_3 and ν_4 bands of CH_4 and tests using laboratory and planetary measurements—I: N_2 (and air) broadening and the Earth atmosphere, *J. Quant. Spectrosc. Radiat. Transfer*, *101*, 284–305.

Tran, H., J.-M. Hartmann, G. Toon, L. R. Brown, C. Frankenberg, T. Warneke, P. Spietz, and F. Hase (2010), The $2\nu_3$ band of CH_4 broadened by N_2 revisited with line-mixing. Consequences for spectroscopic data, laboratory and atmospheric spectra at 1.67 μm, *J. Quant. Spectrosc. Radiat. Transfer*, *111*, 1344–56.

Tran, H., et al. (2015), Infrared light on molecule-molcule and molecule-surface collisions, *Phys. Rev. A*, *92*, 012707.

Truong, G. W., D. A. Long, A. Cygan, D. Lisak, R. D. van Zee, and J. T. Hodges (2013), Comb-linked, cavity ring-down spectroscopy for measurements of molecular transition frequencies at the kHz-level, *J. Chem. Phys.*, *138*, 094201.